



# Electromagnetic wave absorbing properties of SiC/SiO<sub>2</sub> composites with ordered inter-filled structure



Xiaoyan Yuan<sup>b</sup>, Laifei Cheng<sup>a,\*</sup>, Litong Zhang<sup>a</sup>

<sup>a</sup> State Key Laboratory of Solidification Processing, Northwestern Polytechnical University, Xi'an 710072, China

<sup>b</sup> School of Materials Science and Engineering, Shaanxi University of Science and Technology, Xi'an 710021, China

## ARTICLE INFO

### Article history:

Received 18 December 2015

Received in revised form

14 March 2016

Accepted 17 March 2016

Available online 21 April 2016

### Keywords:

SiC/SiO<sub>2</sub> composites

Ordered inter-filled structure

Electromagnetic wave absorption

## ABSTRACT

Silicon carbide/silica (SiC/SiO<sub>2</sub>) monoliths with ordered inter-filled structure were prepared via nanocasting and cold-pressing, using polycarbosilane as precursor and ordered mesoporous silica SBA-15 as template. The SiC grains were incorporated, in form of ordered rodlike arrays, into nanochannels of SBA-15. Their electromagnetic (EM) wave absorbing properties were investigated in X-band, in which SiC acted as EM wave absorber and SiO<sub>2</sub> as transparent matrix. The results indicated that the composites had good EM absorbing properties due to the enhanced dielectric loss resulting from their intrinsic physical properties and special structures. The optimal absorbing properties were determined by impedance match and quarter-wavelength law.

© 2016 Elsevier B.V. All rights reserved.

## 1. Introduction

With the rapid developments of wireless communications and microwave circuits in gigahertz (GHz) range, serious electromagnetic (EM) interference problems have emerged and harmed to the equipments and biological systems [1–4]. At present, radar stealth technology is one of the commanding heights in the military strategy, and the radar monitor frequency focuses on X-band (8.2–12.4 GHz). Therefore, considerable attentions have been aroused and devoted to the EM wave absorbing materials with lightweight and strong absorption at X-band [5–9]. SiC nanomaterials and SiC-based composites, such as SiC nanowires [10], yttria-stabilized zirconia/SiC [11], N–SiC [5], NiO–SiC [12], SiC/CNTs [13,14], vitrified bonded SiC [15], SiCf/SiC [7] and SiC-based ceramic woven fabrics [16], had been reported as the good EM wave absorbing materials, which was because of their excellent chemical stability, good thermal stability and semiconducting properties.

In recent years, ordered mesoporous SBA-15 has been widely used as hard-template and EM wave transparent matrix due to their high ordered structure, good pore-connectivity, good thermal stability and low dielectric constant [17,18]. Liu's group reported the

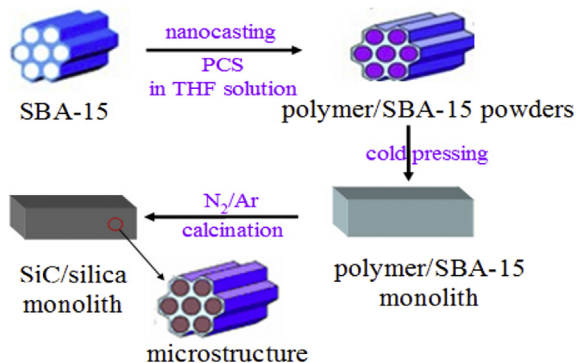
ordered mesostructural C/SBA-15 composites as promising EM wave absorbing materials [19,20]. He et al. synthesized the mesostructure Fe–C/SiO<sub>2</sub> nanocomposites with an enhanced microwave absorbing properties [21]. Above that indicated the ordered inter-filled mesostructure could reflect and scatter the incident EM wave many times and then the EM energy could be completely absorbed in the confined space [22,23]. Meanwhile, these composites had an effective three-dimensional (3D) conductive inter-connection structure, which was conducive to attenuate the EM wave energy [19]. Besides that, the chemical composition of the inter-filled materials was easily modulated to obtain the hybrid composites. Inspired by above results, the composite of the SiC nanoparticles full-filled the nanochannels of SBA-15 will be a good EM wave absorbing material.

On the other hand, Shi et al. [24] and our group [25] had respectively synthesized the SiC powder and monolith with high ordered mesoporous structure, using PCS as preceramic precursor and the SBA-15 as a start template. These reports indicated that PCS had a good ability to fill into the nanochannels of SiO<sub>2</sub> templates. Meanwhile, the PCS-silica powders can easily press into any monoliths without any binder [25,26]. After nanocasting and sintering, the SiC/SiO<sub>2</sub> composites had the ordered inter-filled mesoporous structure, which can effectively attenuate EM wave energy. Therefore, our article presents a competitive and important work.

In present work, the SiC/SiO<sub>2</sub> monolithic composites with ordered mesoporous inter-filled structure were prepared by a simple synthesis route. The influences of the microstructures on EM wave

\* Corresponding author.

E-mail addresses: [xiaoyanyuan0519@163.com](mailto:xiaoyanyuan0519@163.com) (X. Yuan), [chenglf@nwpu.edu.cn](mailto:chenglf@nwpu.edu.cn) (L. Cheng).



**Scheme 1.** Schematic illustration of the ordered inter-filled SiC/SiO<sub>2</sub> composite.

absorption performances were investigated at X-band. The results clearly indicated that the combination of the specific structure and high crystallinity SiC can be contributed to an enhanced microwave absorption property. To find the optimal reflection loss (RL) and matching thickness, the quarter-wavelength thicknesses and impedance match degree plots were constructed and the relevant loss mechanisms were proposed herein.

## 2. Experimental details

### 2.1. Chemicals

Triblock poly(ethylene oxide)-*b*-poly(propylene oxide)-*b*-poly(ethylene oxide) copolymer Pluronic P123 ( $M_w = 5800$ , EO<sub>20</sub>PO<sub>70</sub>EO<sub>20</sub>) was purchased from Sigma-Aldrich. Polycarbosilane (PCS) was obtained from lab of ceramic fiber and composites, National University of Defense Technology, China. Others chemicals were purchased from Shanghai Reagents Co., Ltd. All chemicals were used as received state without any further purification. High-purity argon (99.99%) was used in their as-received state during the ceramic preparation.

### 2.2. Synthesis of mesoporous SBA-15 and SiC/SiO<sub>2</sub> monolithic composites

Mesoporous silica SBA-15 was prepared by hydrothermal synthesis method according to established procedures [17], using P123 as structure directing agent and TEOS as a precursor. A detailed explanation on the synthesis and characterization of the mesoporous SBA-15 were given in the [Support Information \(SI\)](#).

The SiC/SiO<sub>2</sub> monoliths were synthesized by a combined process of nanocasting and cold-pressing. A flow chart of the synthesis procedure was shown in [Scheme 1](#). In a typical process, 4.0 g of SBA-15 was placed in a flask, dried at 150 °C under a vacuum for 4.0 h and cooled down to room temperature (RT), and then added in the solution of 5.0 g PCS and 45.0 ml THF to stir for 6.0 h. After that, the THF solvent was removed under vacuum to generate a powdery mixture. The fine powdery mixtures were obtained by grinding in

an onyx mortar and sieving with the 300 mesh sieve. Subsequently, the powders were equally divided into four parts and each was added into a stainless steel mould to cold-press into a cuboids monolith under a pressure of 10.0 MPa for 2.0 min. Finally, the polymer/SiO<sub>2</sub> monolith was transferred into a horizontal ceramic tube furnace and subjected to the thermal treatment in Ar atmosphere at  $x$  °C ( $x = 1200, 1300, 1400$  or  $1500$ ) for 2 h with a heating rate of 1 °C min<sup>-1</sup>, to generate SiC/SiO<sub>2</sub> monolithic ceramic. The monoliths pyrolyzed at different temperatures were denoted as SiC/SiO<sub>2</sub>-1200, SiC/SiO<sub>2</sub>-1300, SiC/SiO<sub>2</sub>-1400 and SiC/SiO<sub>2</sub>-1500, respectively.

### 2.3. Characterization

Powder small-angle X-ray diffraction (SA-XRD) and wide-angle X-ray diffraction (WA-XRD) patterns were achieved using a Philipps X'Pert PRO X-ray diffraction system (Cu K $\alpha$  radiation, 0.15406 nm). The surface morphology was investigated by a field emission scanning electron microscope (FE-SEM, S4700). Transmission electron microscopy (TEM) measurement was conducted on a FEI T20 microscope operated at 200 kV. Nitrogen adsorption-desorption isotherm measurements were performed on a Micromeritics ASAP 2020 volumetric adsorption analyzer at -196 °C. The mechanical compressive strength of the monoliths was evaluated using a universal tensile testing machine (SHIMADZU Universal Testing Machine AGS-X 5kN) at room temperature. Direct current (DC) conductivity was performed with a standard two lines method using the DC Source (Precise Current Source by Keithley, 6220, USA). The dielectric properties were measured by a vector network analyzer (VNA, MS4644A, Anritsu, Atsugi, Japan) in X-band (8.2–12.4 GHz) using the wave-guide method. The as-prepared sample was placed vertically in the center of test chamber during measurement.

## 3. Results and discussion

### 3.1. Morphology and microstructure

The synthetic approach for the ordered mesoporous inter-filled SiC/SiO<sub>2</sub> monoliths was shown in [Scheme 1](#). The microstructures of the SBA-15 were shown in [Fig. S1](#) in the SI. The SBA-15 exhibited 2-D *P6mm* hexagonal symmetry with a specific surface area of 573 m<sup>2</sup> g<sup>-1</sup> and an average pore diameter of 8.9 nm (shown in [Table 1](#)). These results indicated that the SBA-15 had good ordered mesoporous structure, high specific surface area and narrow pore-size distribution.

The typical cross-section SEM images of SiC/SiO<sub>2</sub> monoliths were shown in [Fig. 1](#). The samples of SiC/SiO<sub>2</sub>-1200, SiC/SiO<sub>2</sub>-1300 and SiC/SiO<sub>2</sub>-1400 all exhibited interconnected particles with a uniform size of about 1.0  $\mu$ m (shown in [Fig. 1a–c](#)). The morphologies of these monoliths were similar to that of the SBA-15, which confirmed that the SiC grains were restricted into channels of the SBA-15 [25,27]. When the calcination temperature was 1500 °C, the as-prepared composite was constructed from unconnected particles (shown in [Fig. 1d](#)). Meanwhile, there were many big pores in

**Table 1**  
Textural data of the samples.

Sample	$S_{BET}$ (m <sup>2</sup> g <sup>-1</sup> )	Pore volume (cm <sup>3</sup> g <sup>-1</sup> )	Pore size (nm)	Compression strength (MPa, RT)
SBA-15	573.0	1.0	8.9	–
SiC/SiO <sub>2</sub> -1200	25.3	–	–	43.8
SiC/SiO <sub>2</sub> -1300	38.5	0.1	3.8	52.0
SiC/SiO <sub>2</sub> -1400	60.7	0.13	4.0	68.5
SiC/SiO <sub>2</sub> -1500	15.6	–	–	39.2

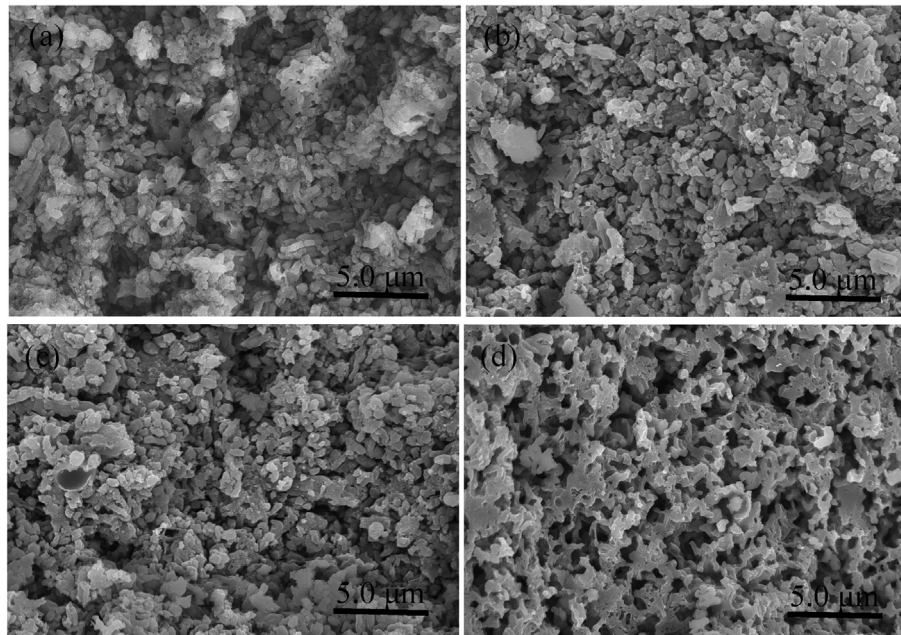


**Fig. 1.** Cross-section SEM images of the SiC/SiO<sub>2</sub>-1200 (a), SiC/SiO<sub>2</sub>-1300 (b), SiC/SiO<sub>2</sub>-1400 (c) and SiC/SiO<sub>2</sub>-1500 (d), respectively.

the composite. The possible reason was the template SiO<sub>2</sub> reacted with free carbon from PCS pyrolysis at 1500 °C to produce and then escape some small-molecule gases, such as SiO, CO, CO<sub>2</sub> and so on, to form these macropores. Meanwhile, the SiC crystals were growth

at 1500 °C to cause the ordered structure collapse. Therefore, the ordered mesoporous inter-filled structure was also destroyed at 1500 °C.

Evidence of the maintenance of ordered mesoporous inter-filled

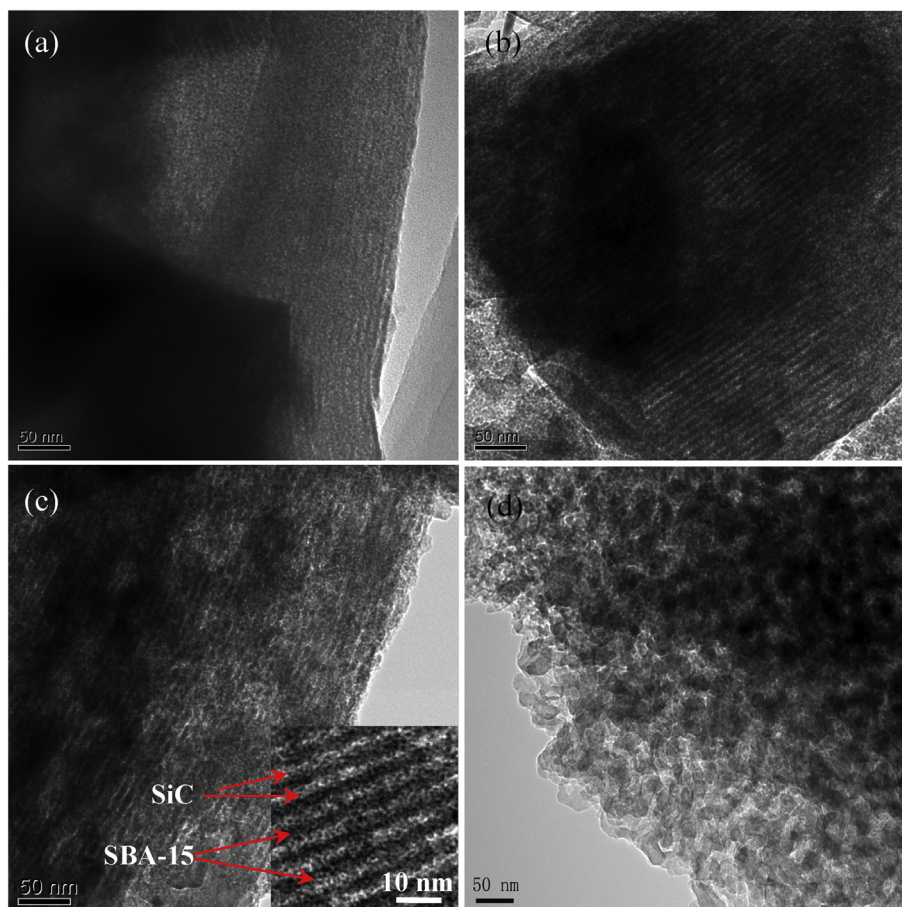


**Fig. 2.** TEM images of the SiC/SiO<sub>2</sub>-1200 (a), SiC/SiO<sub>2</sub>-1300 (b), SiC/SiO<sub>2</sub>-1400 (c) and SiC/SiO<sub>2</sub>-1500 (d), respectively. The inset in (c) is the corresponding HR-TEM image.

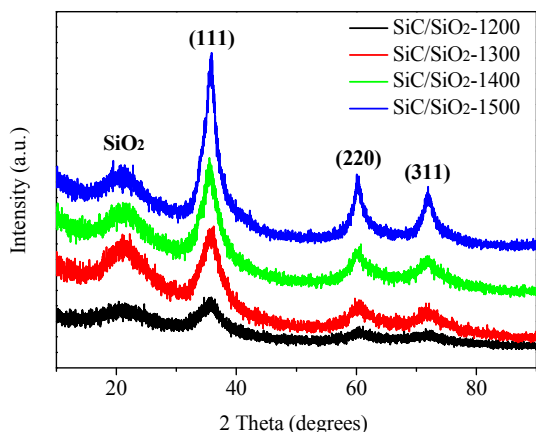


Fig. 3. WA-XRD patterns of the SiC/SiO<sub>2</sub> composites.

structure for the SiC/SiO<sub>2</sub> samples was also provided by TEM images. As shown in Fig. 2a–c, the composites of SiC/SiO<sub>2</sub>-1200, SiC/SiO<sub>2</sub>-1300 and SiC/SiO<sub>2</sub>-1400 exhibited characteristic cylindrically rod-like arrays in large domains, as evident in the inset of high-resolution TEM (HT-TEM) image of SiC/SiO<sub>2</sub>-1400 shown in Fig. 2c. The inter-filled SiC nanoparticles and SiO<sub>2</sub> matrix were in tight contact with each other and no cavities. These results indicated that the nanochannels of the SBA-15 were almost filled by SiC grains, which had been proved that the ordered mesoporous SiC powder and monolith were obtained after removing the SiO<sub>2</sub>

[24,25]. As shown in Fig. 2d, the ordered structure was destroyed at 1500 °C, which was consisted with that of the SEM. Therefore, through the polymer-to-ceramic conversion process and the calcination temperature less than 1500 °C, the ordered mesoporous inter-filled arrays can be conserved for SiC/SiO<sub>2</sub> monolithic composites.

Fig. 3 showed the typical WA-XRD patterns of the SiC/SiO<sub>2</sub> composites. It was clear to see that the crystallinity of the as-prepared composites increased with the increasing calcination temperature. The diffraction peaks in each pattern were indexed to the  $\beta$ -SiC according to the JCPDS 01-1119. Using Scherrer's formula, the SiC grain sizes were estimated to be 0.4, 4.2, 6.3 and 18.4 nm for SiC/SiO<sub>2</sub>-1200, SiC/SiO<sub>2</sub>-1300, SiC/SiO<sub>2</sub>-1400 and SiC/SiO<sub>2</sub>-1500. We can see that the size of SiC crystals at 1500 °C were clearly bigger than the channels size of SBA-15, as a further evidence for the disordered structure of SiC/SiO<sub>2</sub>-1500. Moreover, a broad band at 21–23° existed in each pattern was related with SiO<sub>2</sub> suggesting its amorphous nature.

Nitrogen isotherms adsorption-desorption isotherms and pore-size distributions of the SiC/SiO<sub>2</sub> composites were shown in the SI. From Fig. S2a, the isotherms of SiC/SiO<sub>2</sub>-1200 and SiC/SiO<sub>2</sub>-1500 didn't show the hysteric loop characteristic in each curve, which was due to the amorphous SiC were fully filled mesopores of the SBA-15 for SiC/SiO<sub>2</sub>-1200 and the mesostructure totally damaged at high temperature for SiC/SiO<sub>2</sub>-1500. Their corresponding pore size distributions also proved the above results. However, a relatively obvious hysteric loop was exhibited in the each isotherm of the SiC/SiO<sub>2</sub>-1300 and SiC/SiO<sub>2</sub>-1400. Base on models of pore-filling mechanisms [28], the above phenomenon indicated SiC

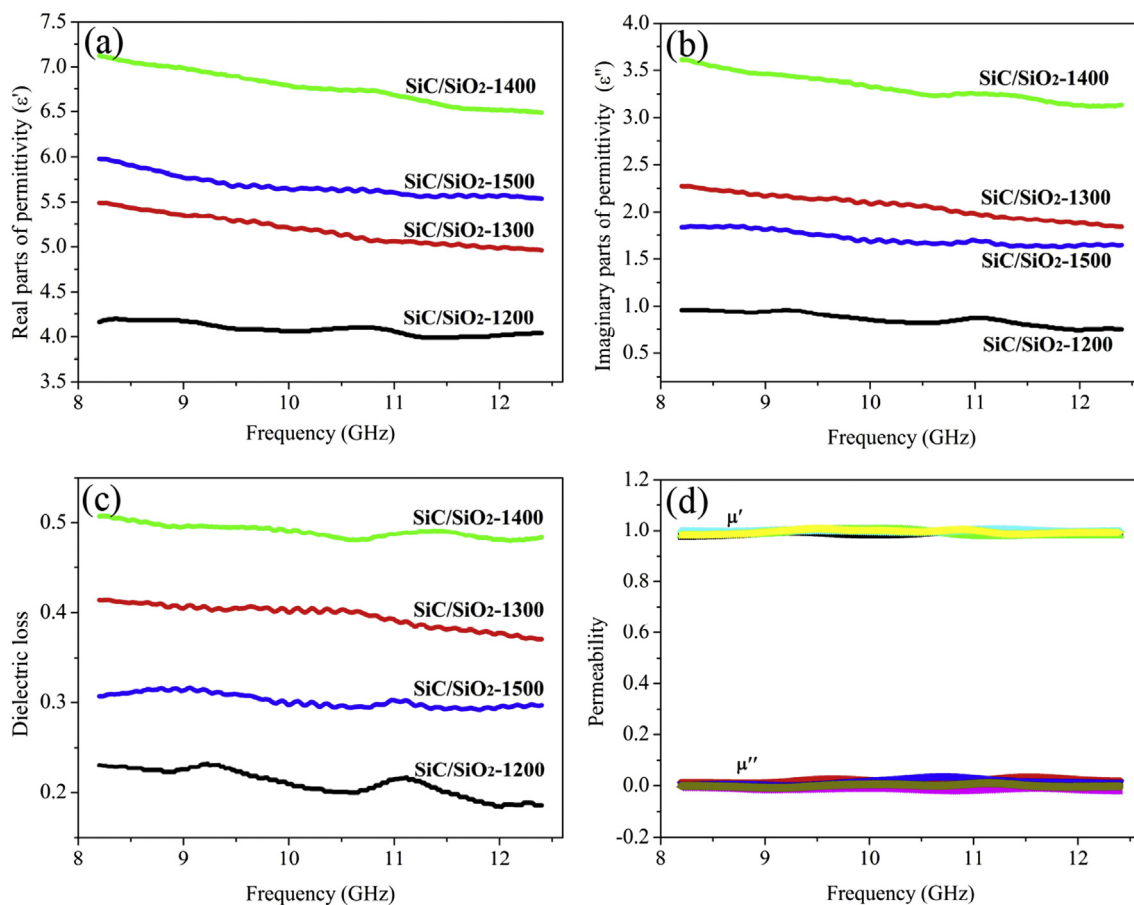


Fig. 4. The real (a) and imaginary parts (b) of complex permittivity, the dielectric loss (c) and the complex permeability (d) as a function of frequency for the SiC/SiO<sub>2</sub> composites.

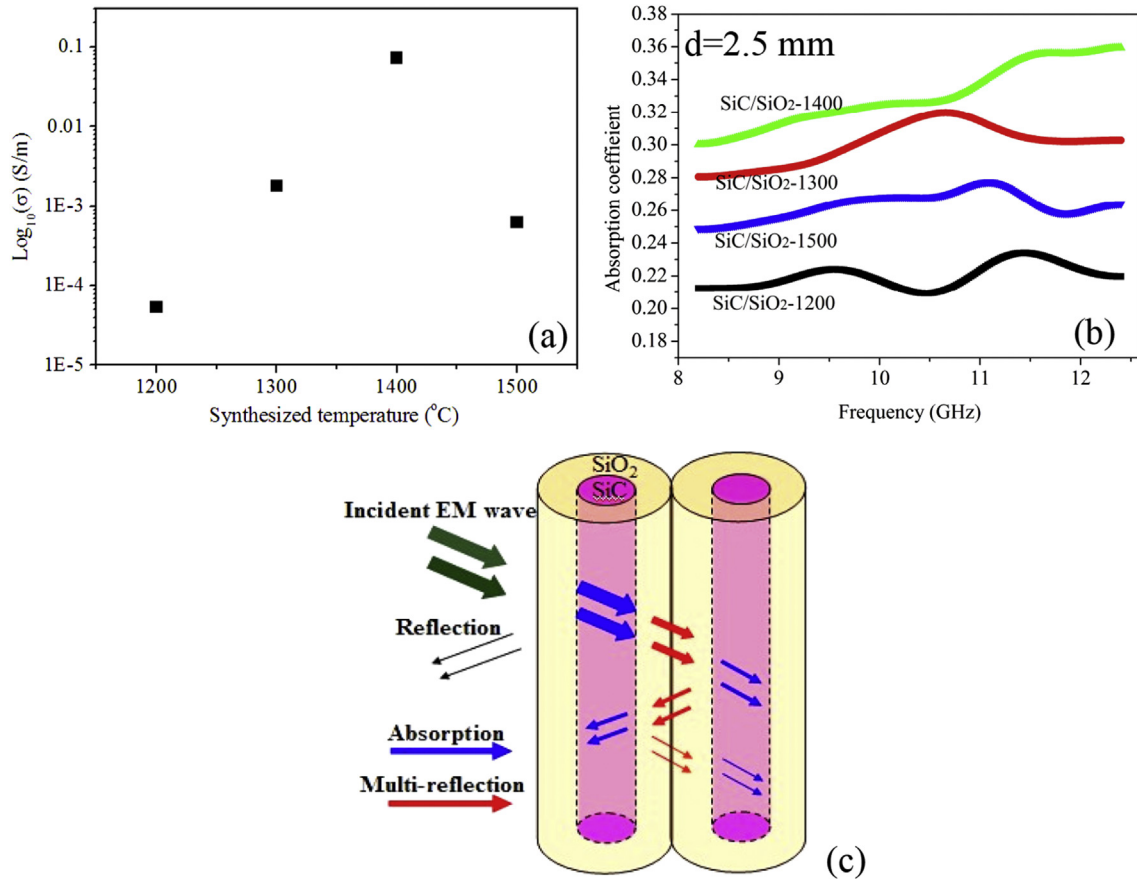


Fig. 5. The DC conductivity (a), absorption coefficients (b) and schematic diagram representing the EM wave attenuate mechanisms (c) for the SiC/SiO<sub>2</sub> composites.

nanocrystals filled inside nanochannels of the SBA-15. The specific BET surface areas and average pore sizes of the SiC/SiO<sub>2</sub> composites were shown in Table 1. Although the equal PCS inter-filled materials, the mesopore data of SiC/SiO<sub>2</sub> composites had a little difference. The probable reasons were that the mass of SiC from PCS pyrolyzed at different temperatures had a little difference and the pores formed by the accumulative SiC crystals at high temperatures to increase the specific BET surface areas. In addition, the average value of compressive strength for SiC/SiO<sub>2</sub> composites increased firstly and then decrease with the increasing calcination temperature (shown in Table 1). The enhancement for the SiC/SiO<sub>2</sub>-1400 was mainly due to the high crystallinity and compactness. However, the reduction for the SiC/SiO<sub>2</sub>-1500 was mainly due to the low compactness caused by the big pores.

### 3.2. EM wave absorption properties

The mesoporous silica SBA-15 has small dielectric constant ( $\epsilon' = 3.9\text{--}4.2$  and  $\epsilon'' = 0\text{--}0.2$ ) at GHz frequency range [18]. As known to all, the real part ( $\epsilon'$ ) and imaginary part ( $\epsilon''$ ) of relative complex permittivity ( $\epsilon_r = \epsilon' - j\epsilon''$ ) represent the energy storage and dissipation capability, respectively. So the SBA-15 is a good EM wave transparent matrix. In Fig. 4a and b, the values of  $\epsilon'$  and  $\epsilon''$  increased firstly and then decreased. The values of  $\epsilon'$  and  $\epsilon''$  for the SiC/SiO<sub>2</sub>-1400 were the highest. The dielectric loss ( $\tan\delta_E = \epsilon''/\epsilon'$ ) of the SiC/SiO<sub>2</sub> composites were illustrated in Fig. 4c. The  $\tan\delta_E$  values of the SiC/SiO<sub>2</sub>-1400 were higher than others, which indicated the SiC/SiO<sub>2</sub>-1400 had stronger EM wave loss abilities. Moreover, the real part ( $\mu'$ ) and imaginary part ( $\mu''$ ) of relative complex permeability

( $\mu_r = \mu' - j\mu''$ ) of the SiC/SiO<sub>2</sub> composites were all close to 1 and 0 in this case (shown in Fig. 4d), due to their non-magnetic properties.

The ordered inter-filled mesoporous structures and SiC nanocrystals interaction had numerous complicated interfaces, at which EM radiation with charges can enhance the polarization capability [10,29]. Therefore, this special structure and complicated interfaces led to the high  $\epsilon'$  for the SiC/SiO<sub>2</sub>-1400. As the SBA-15 with pore-connectivity, the complex conductance paths were easily formed by the SiC grains to increase the electric conductivity. This was beneficial to the high  $\epsilon''$  for the SiC/SiO<sub>2</sub>-1400. Although the SiC/SiO<sub>2</sub>-1500 had high crystallinity, the particular structure was destroyed and led to their  $\epsilon'$  and  $\epsilon''$  values all decrease (shown in Fig. 4a and b). Therefore, the ordered inter-filled structure of the composites in this case was a main contributor for depleting EM wave energy.

It is well known that  $\epsilon''$  has a similar tendency with conductivity at the same temperature,  $\epsilon'' \approx \sigma/2\pi\epsilon_0 f$ . As a function of synthesized temperature, DC conductivity of the SiC/SiO<sub>2</sub> composites was shown in Fig. 5a, which had the same tendency with the  $\epsilon''$ . In our case, the DC conductivities of samples were  $5.46 \times 10^{-5}$  for SiC/SiO<sub>2</sub>-1200,  $1.8 \times 10^{-3}$  for SiC/SiO<sub>2</sub>-1300,  $7.25 \times 10^{-2}$  for SiC/SiO<sub>2</sub>-1400 and  $6.2 \times 10^{-4}$  for SiC/SiO<sub>2</sub>-1500, respectively. The SiC nanoparticles with high crystallinity and ordered connective structure could increase the sample's conductivity. And the electric conductance paths were destroyed at 1500 °C to cause the low conductivity for the SiC/SiO<sub>2</sub>-1500.

From the dielectric measurement, the S-parameters ( $S_{11}$  and  $S_{21}$ ) were obtained. According to S-parameters, the reflection coefficient (R), absorption coefficient (A), and transmission coefficient (T) were

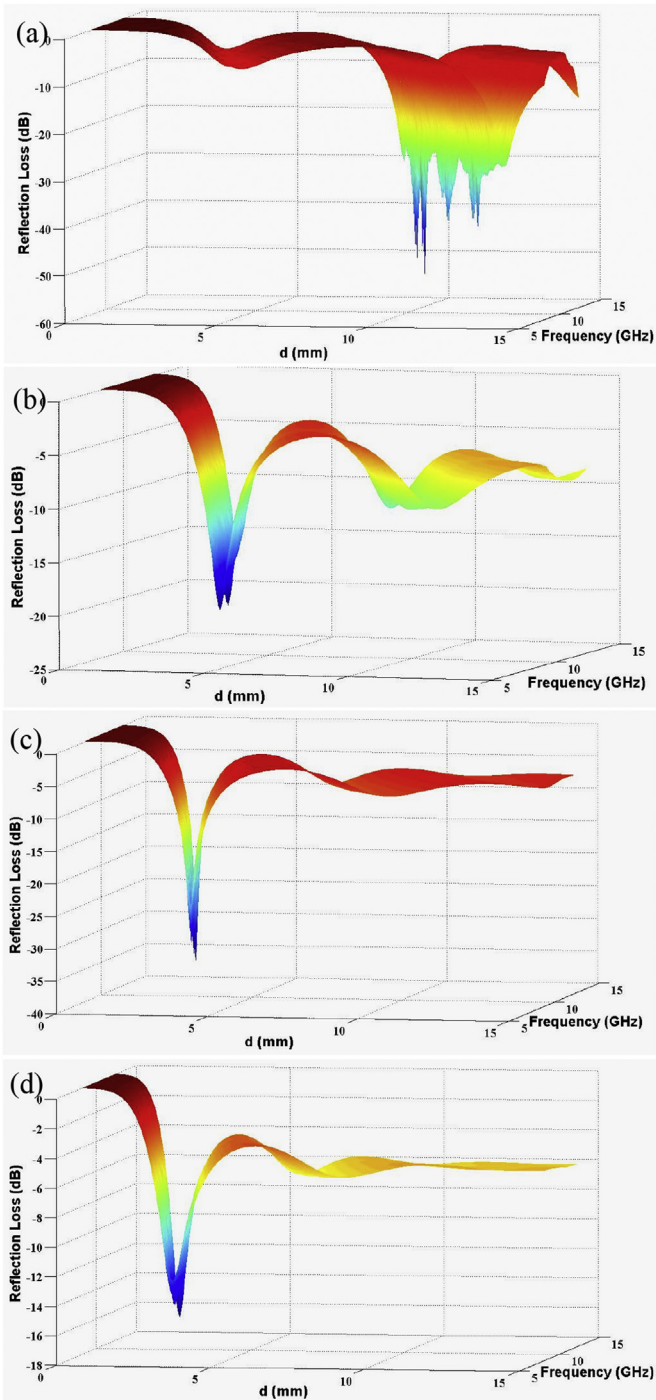


Fig. 6. Three-dimensional (3-D) images of the calculated RL for the SiC/SiO<sub>2</sub>-1200 (a), SiC/SiO<sub>2</sub>-1300 (b), SiC/SiO<sub>2</sub>-1400 (c) and SiC/SiO<sub>2</sub>-1500 (d), respectively.

calculated [30]. Here R and T were primarily given as  $R = |S_{11}|^2$  and  $T = |S_{21}|^2$ , respectively. We can use the relation  $A + R + T = 1$  to obtain A from the results of R and T. Variation of absorption coefficients of the SiC/SiO<sub>2</sub> composites with a thickness of 2.5 mm were given in Fig. 5b. It was clear to see that the SiC/SiO<sub>2</sub>-1400 had a relatively higher absorption coefficient than others. The EM wave absorbing mechanism was indicated by a schematic diagram (shown in Fig. 5c). The incident EM waves were confined within the ordered inter-filled mesostructure and multiple reflections induced the energy dissipation occurring in many different sites [20,31].

Therefore, the ordered inter-filled mesostructure was beneficial to EM wave attenuation.

To predict the EM wave absorption of the SiC/SiO<sub>2</sub> composites, the RL was calculated by the following equations: [32]

$$RL(\text{dB}) = 20 \log_{10} |(Z_{in} - Z_0)/(Z_{in} + Z_0)| \quad (1)$$

$$Z_{in} = Z_0 \sqrt{\mu_r/\epsilon_r} \tanh\left(j \frac{2\pi f d}{c} \sqrt{\mu_r^* \epsilon_r^*}\right) \quad (2)$$

where  $d$  is the absorption layer thickness,  $c$  is the velocity of light and  $Z_{in}$  is the normalized input impedance, the EM absorption layer, respectively. According to Eqn (1) and (2), 3-D images of RL, thickness and frequency for the SiC/SiO<sub>2</sub> composites were illustrated in Fig. 6. Due to the destructive interference, the plots of each composite exhibited the undulate shape as the thickness. The destructive interference is caused by the inverse phase (phase difference of 180°) of the reflection EM wave from the upper and bottom surfaces of the materials [33]. This is so-called the quarter-wavelength principle:  $d = (n/4)\lambda = (n/4)\lambda_0 / (|\epsilon_r||\mu_r|)^{1/2}$  ( $n = 1, 3, 5, 7 \dots$ ), where  $\lambda_0$  is the free space wavelength,  $|\epsilon_r|$  and  $|\mu_r|$  are the moduli of  $\epsilon_r$  and  $\mu_r$ , respectively. Therefore, combining the absorbing ability of material itself and destructive interference caused by the thickness of material should be the main path to loss EM wave energy. Compared the images in Fig. 6, it was clear to see that the SiC/SiO<sub>2</sub>-1400 (shown in Fig. 6c) had stronger absorbing ability than others.

To further discussion the EM absorbing property, the SiC/SiO<sub>2</sub>-1400 was taken as an example. Its 2-D map of RL was shown in Fig. 7a, in which the optimal absorptions were observed at the thickness around 3.0 mm. The detailed RL at different thicknesses was shown in Fig. 7b. With increasing the thickness from 2.5 mm to 3.25 mm, the peak of RL shifted to lower frequency. When the thickness was 2.75 mm, the minimum RL value reached -52 dB at 10.8 GHz. And the thick layer of 3.0 mm, the effective absorption bandwidth (RL < -10 dB) covered the whole X-band, at which the 90% of incident EM wave can be attenuated. Moreover, the vertical dot lines from the RL peaks were extended and crossed with the  $(1/4)\lambda$  curve in Fig. 7d and the crossover points were denoted by the asteroid dots. We can see that the thicknesses of all the asteroid dots located on the  $(1/4)\lambda$  curve were scarcely less with that of composite. Therefore, the attenuation of EM wave absorbing material could be modulated simply by manipulating the material's thickness for applications at different frequency bands.

Impedance match is an important factor too. Cao et al. had studied the matching and mismatching on absorbing performance and obtained the design rules for single layer absorption materials [34]. In this case, the magnetic loss was about zero, due to the composites' non-magnetic properties. The attenuation was mainly caused by dielectric loss. Meanwhile, Ma et al. had pointed out that  $\Delta$  ( $\Delta = |\sinh^2(Kfd) - M|$ ) represented the impedance matching degree [35], where K and M are determined by the complex permittivity and permeability. When  $\Delta$  tends to zero, it means that the material has a good impedance match and a good EM wave absorption will be obtained at the corresponding thickness. Fig. 7c showed the  $\Delta$  as function as thickness and frequency for the SiC/SiO<sub>2</sub>-1400. From that, the thicknesses were around 3.0 mm for the good impedance match, which was consistent with the above results. Therefore, the optimal absorbing properties should obey the quarter-wavelength principle and impedance matching degree.

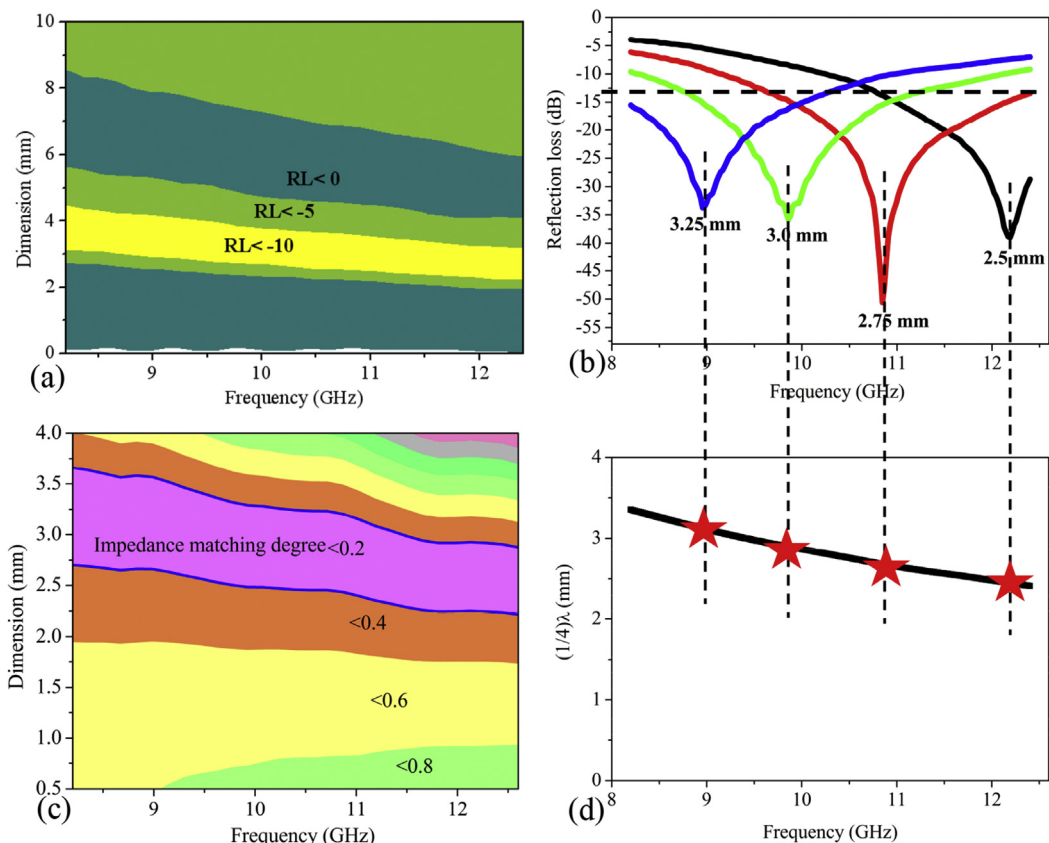


Fig. 7. The SiC/SiO<sub>2</sub>-1400: (a) two-dimensional (2-D) color map of RL; (b) RL values at the various thicknesses; (c) 2-D color map of impedance match degree; (d) the  $(1/4)\lambda$  curve. The vertical dashed lines in (b) from RL peaks at different thicknesses to cross with  $(1/4)\lambda$  curve in (d), and the crossover points are indicated by the asteroid dots.

#### 4. Conclusions

In summary, an effect EM wave absorbing material of SiC/SiO<sub>2</sub> monolith with ordered inter-filled mesostructure was prepared by nanocasting and cold-pressing. In X-band, the SiC/SiO<sub>2</sub>-1400 displayed a minimum RL of  $-52.0$  dB at 10.8 GHz and effective absorption bandwidth (RL  $< -10$  dB) exceed the whole X-band. The EM wave attenuation was contributed to their special structures and intrinsic physical properties. Meanwhile, the optimal thickness was obeyed the impedance match law and destructive interference. Therefore, such ordered inter-filled mesostructural SiC/SiO<sub>2</sub> composites will be suitable as EM wave absorption materials for the application at high-temperature.

#### Acknowledgments

This work is supported by the funds of the State Key Laboratory of Solidification Processing in NWP (SKLSP201503) and the Natural Science Foundation of China (51502164).

#### Appendix A. Supplementary data

Supplementary data related to this article can be found at <http://dx.doi.org/10.1016/j.jallcom.2016.03.309>.

#### References

[1] X.W. Yin, L. Kong, L.T. Zhang, L.F. Cheng, N. Travitzky, P. Greil, Electromagnetic properties of Si-C-N based ceramics and composites, *Int. Mater. Rev.* 59 (2014) 326–355.  
 [2] Y. Mu, W.C. Zhou, Y. Hu, D.H. Ding, F. Luo, Y.C. Qing, Enhanced microwave

absorbing properties of 2.5D SiCf/SiC composites fabricated by a modified precursor infiltration and pyrolysis process, *J. Alloys Compd.* 637 (2015) 261–266.  
 [3] H.J. Yang, W.Q. Cao, D.Q. Zhang, T.J. Su, H.L. Shi, W.Z. Wang, J. Yuan, M.S. Cao, NiO hierarchical nanorings on SiC: enhancing relaxation to tune microwave absorption at elevated temperature, *ACS Appl. Mater. Interfaces* 7 (2015) 7073–7077.  
 [4] L.Q. Chen, X.W. Yin, X.M. Fan, M. Chen, X.K. Ma, L.F. Cheng, L.T. Zhang, Mechanical and electromagnetic shielding properties of carbon fiber reinforced silicon carbide matrix composites, *Carbon* 95 (2015) 10–19.  
 [5] Y.K. Dou, J.B. Li, X.Y. Fang, H.B. Jin, M.S. Cao, The enhanced polarization relaxation and excellent high-temperature dielectric properties of N-doped SiC, *Appl. Phys. Lett.* 104 (2014) 052102.  
 [6] W.L. Song, X.T. Guan, L.Z. Fan, W.Q. Cao, C.Y. Wang, M.S. Cao, Tuning three-dimensional textures with graphene aerogels for ultra-light flexible graphene/texture composites of effective electromagnetic shielding, *Carbon* 93 (2015) 151–160.  
 [7] D.H. Ding, Y.M. Shi, Z.H. Wu, W.C. Zhou, F. Luo, J. Chen, Electromagnetic interference shielding and dielectric properties of SiCf/SiC composites containing pyrolytic carbon interphase, *Carbon* 60 (2013) 552–555.  
 [8] M.S. Cao, X.X. Wang, W.Q. Cao, J. Yuan, Ultrathin graphene: electrical properties and highly efficient electromagnetic interference shielding, *J. Mater. Chem. C* 3 (2015) 6589–6599.  
 [9] M.S. Cao, J. Yang, W.L. Song, D.Q. Zhang, B. Wen, H.B. Jin, Z.L. Hou, J. Yuan, Ferroferric oxide/multiwalled carbon nanotube vs polyaniline/ferroferric oxide/multiwalled carbon nanotube multiheterostructures for highly effective microwave absorption, *ACS Appl. Mater. Interfaces* 4 (2012) 6949–6956.  
 [10] S.C. Chiu, H.C. Yu, Y.Y. Li, High electromagnetic wave absorption performance of silicon carbide nanowires in the gigahertz range, *J. Phys. Chem. C* 114 (2010) 1947–1952.  
 [11] X.W. Yin, Y.Y. Xue, L.T. Zhang, L.F. Cheng, Electromagnetic absorption and interference shielding properties of porous yttria-stabilized zirconia/silicon carbide composites, *Ceram. Int.* 38 (2012) 2421–2427.  
 [12] H.J. Yang, M.S. Cao, Y. Li, H.L. Shi, Z.L. Hou, X.Y. Fang, H.B. Jin, W.Z. Wang, J. Yuan, Enhanced dielectric properties and excellent microwave absorption of SiC powders driven with NiO nanorings, *Adv. Opt. Mater.* 2 (2014) 214–219.  
 [13] J.K. Yuan, W.L. Li, S.H. Yao, Y.Q. Lin, A. Sylvestre, J.B. Bai, High dielectric permittivity and low percolation threshold in polymer composites based on SiC-carbon nanotubes micro/nanohybrid, *Appl. Phys. Lett.* 98 (2011) 032901–032903.

- [14] H.L. Zhu, Y.J. Bai, R. Liu, N. Lun, Y.X. Qi, F.D. Han, J.Q. Bi, In situ synthesis of one-dimensional MWCNT/SiC porous nanocomposites with excellent microwave absorption properties, *J. Mater. Chem.* 21 (2011) 13581–13587.
- [15] Q.C. Meng, Z.H. Li, Y.M. Zhu, D.D. Feng, H.Y. Tan, Mechanical and X-band dielectric properties of vitrified bonded SiC composites, *Mater. Des.* 92 (2016) 18–22.
- [16] E. Tan, Y. Kagawa, A.F. Dericioglu, Electromagnetic wave absorption potential of SiC-based ceramic woven fabrics in the GHz range, *J. Mater. Sci.* 44 (2009) 1172–1179.
- [17] D.Y. Zhao, J.L. Feng, Q.S. Huo, N. Melosh, G.H. Fredrickson, B.F. Chmelka, G.D. Stucky, Triblock copolymer syntheses of mesoporous silica with periodic 50 to 300 Angstrom pores, *Science* 279 (1998) 548–552.
- [18] W. Shan, L. Chen, Y. Chu, F.P. Zhao, G.Z. Liang, A.J. Gu, L. Yuan, Synthesis of a fully capped mesoporous silica and its hybrids with extremely low dielectric constant and loss, *Micropor. Mesopor. Mater.* 176 (2013) 199–208.
- [19] J.C. Wang, C.S. Xiang, Q. Liu, Y.B. Pan, J.K. Guo, Ordered mesoporous carbon/fused silica composites, *Adv. Funct. Mater.* 18 (2008) 2995–3002.
- [20] J.C. Wang, H. Zhou, J.D. Zhuang, Q. Liu, Influence of spatial configurations on electromagnetic interference shielding of ordered mesoporous carbon/ordered mesoporous silica/silica composites, *Sci. Rep.* 3 (2013) 3252–3257.
- [21] J.H. Zhou, J.P. He, G.X. Li, T. Wang, D. Sun, X.C. Ding, J.Q. Zhao, S.C. Wu, Direct incorporation of magnetic constituents within ordered mesoporous carbon-silica nanocomposites for highly efficient electromagnetic wave absorbers, *J. Phys. Chem. C* 114 (2010) 7611–7617.
- [22] W.L. Song, M.S. Cao, L.Z. Fan, M.M. Lu, Y. Li, C.Y. Wang, H.F. Ju, Highly ordered porous carbon/wax composites for effective electromagnetic attenuation and shielding, *Carbon* 77 (2014) 130–142.
- [23] H. Zhou, J.D. Zhuang, Q. Yan, Q. Liu, Facile preparation and high microwave absorption of C/SiO<sub>2</sub> composites with an ordered inter-filled string mesostructure, *Mater. Lett.* 85 (2012) 117–119.
- [24] Y.F. Shi, Y. Meng, D.H. Chen, S.J. Cheng, P. Chen, H.F. Yang, Y. Wan, D.Y. Zhao, Highly ordered mesoporous silicon carbide ceramics with large surface areas and high stability, *Adv. Funct. Mater.* 16 (2006) 561–567.
- [25] X.Y. Yuan, J.W. Lü, X.B. Yan, L.T. Hu, Q.J. Xue, Preparation of ordered mesoporous silicon carbide monoliths via preceramic polymer nanocasting, *Micropor. Mesopor. Mater.* 142 (2011) 754–758.
- [26] X.Y. Yuan, L.F. Cheng, Y.J. Zhang, S.W. Guo, L.T. Zhang, Fe-doped SiC/SiO<sub>2</sub> composites with ordered inter-filled structure for effective high-temperature microwave attenuation, *Mater. Des.* 92 (2016) 563–570.
- [27] X.B. Yan, L. Gottardo, S. Bernard, P. Dibandjo, A. Brioude, H. Moutaabbid, P. Miele, Ordered mesoporous silicoboron carbonitride materials via preceramic polymer nanocasting, *Chem. Mater.* 20 (2008) 6325–6334.
- [28] H.Q. Ly, R. Taylor, R.J. Day, Conversion of polycarbosilane (PCS) to SiC-based ceramic part II. pyrolysis and characterization, *J. Mater. Sci.* 6 (2001) 4045–4057.
- [29] J. Liu, W.Q. Cao, H.B. Jin, J. Yuan, D.Q. Zhang, M.S. Cao, Enhanced permittivity and multi-region microwave absorption of nanoneedle-like ZnO in the X-band at elevated temperature, *J. Mater. Chem. C* 3 (2015) 4670–4677.
- [30] N.F. Colaneri, L.W. Shaklette, EMI shielding measurements of conductive polymer blends, *IEEE Trans. Instrum. Meas.* 41 (1992) 291–297.
- [31] H. Zhou, J.H. Wang, J.D. Zhuang, Q. Liu, A covalent route for efficient surface modification of ordered mesoporous carbon as high performance microwave absorbers, *Nanoscale* 5 (2013) 12502–12511.
- [32] J.H. Kwon, J.Y. Shin, J.H. Oh, The microwave absorbing and resonance phenomena of Y-type hexagonal ferrite microwave absorbers, *J. Appl. Phys.* 75 (1994) 6109–6111.
- [33] A.N. Yusoff, M.H. Abdullah, S.H. Ahmad, S.F. Jusoh, A.A. Mansor, S.A.A. Hamid, Electromagnetic and absorption properties of some microwave absorbers, *J. Appl. Phys.* 92 (2002) 876–882.
- [34] M.S. Cao, R.R. Qin, C.J. Qiu, J. Zhu, Matching design and mismatching analysis towards radar absorbing coatings based on conducting plate, *Mater. Des.* 24 (2003) 391–396.
- [35] Z. Ma, Y. Zhang, C.T. Cao, J. Yuan, Q.F. Liu, J.B. Wang, Attractive microwave absorption and the impedance match effect in zinc oxide and carbonyl iron composite, *Phys. B* 406 (2011) 4620–4624.